Highly thermally stable polyhedral oligomeric silsesquioxane based on diacetal-functionalized polybenzoxazine nanocomposites

Mohsin Ejaz [a], Mohamed Gamal Mohamed [a,b,*], Wei-Chun Huang [a], Yang-Chin Kao [a], Wei-Cheng Chen [a], Shiao-Wei Kuo [a,c,*]

[a] Department of Materials and Optoelectronic Science, Center for Functional Polymers and Supramolecular Materials, National Sun Yat-Sen University, Kaohsiung 804, Taiwan
[b] Department of Chemistry, Faculty of Science, Assiut University, Assiut 71515, Egypt
[c] Department of Medicinal and Applied Chemistry, Kaohsiung Medical University, Kaohsiung 807, Taiwan

ABSTRACT

An increasing number of high-performance industries are prioritizing the use of polymeric materials with exceptional thermal stability to support long-term advancements toward a more sustainable future. In this study, we first synthesized an allyl-functionalized benzoxazine (BZ) with a diacetal structure by reacting 4,4′-(2,4,8,10-tetraoxaspiro[5.5]undecane-3,9-diyl)diphenol (ACE) with allylamine in the presence of paraformaldehyde to obtain ACE-BZ monomer. Highly thermally stable organic-inorganic benzoxazines were subsequently prepared through a hydrosilylation reaction of ACE-BZ with double-decker silsesquioxane (DDSQ) and octakis(dimethylsilyloxy)octasilsesquioxane (ODMS-POSS), yielding DDSQ-ACE-BZ and POSS-ACE-BZ polymer networks, respectively. The chemical structures of ACE-BZ, DDSQ-ACE-BZ, and POSS-ACE-BZ were confirmed using FTIR, ^{1}H NMR, and ^{13}C NMR spectroscopy; respectively. The thermal curing peaks, ring-opening polymerization (ROP) behavior, and thermal stability properties of the ACE-BZ, DDSQ-ACE-BZ, and POSS-ACE-BZ were analyzed using differential scanning calorimetry (DSC), FTIR and thermogravimetric analysis (TGA). After thermal curing, the thermal stability (T_{d10}, char yields) of poly(ACE-BZ), poly(DDSQ-ACE-BZ), and poly(POSS-ACE-BZ) were (435 °C, 46 wt%), (544 °C, 75 wt%), and (510 °C, 74 wt%), respectively. Notably, poly(DDSQ-ACE-BZ) demonstrated superior thermal stability compared to poly(POSS-ACE-BZ), primarily attributed to the inherently higher thermal stability of the rigid DDSQ moiety relative to POSS. Based on our current understanding, the DDSQ-based polybenzoxazine resin discussed in this study demonstrates the highest thermal stability that has been documented so far.

1. Introduction

The increasing demand for strong, durable, and lightweight materials in various commercial sectors has led the scientific community to focus extensively on advanced material research [1–3]. High-performance thermosetting polymers are particularly noteworthy due to their exceptional mechanical and thermal properties and low weight, making them suitable for numerous contemporary applications [4–6]. From these materials, cyanate esters, polyurethanes, polyimides epoxies, and phenolics are of significant importance [7–10]. Benzoxazine (BZ) is a heterocyclic compound characterized by the presence of oxygen and nitrogen atoms. It can be synthesized via the Mannich condensation

reaction, which involves the primary amine, the phenolic compound, and formaldehyde derivatives [11,12]. Upon exposure to elevated temperatures, the oxazine units undergo thermal curing to form polybenzoxazines (PBZ), a novel class of thermosetting materials capable of forming inter- and intramolecular hydrogen bonds without the need for additional curing agents or catalysts [13–16].

Polybenzoxazines (PBZs) have garnered considerable attention from both academic and industrial sectors due to their outstanding properties, which include low surface free energy, high adhesive strength, minimal volumetric shrinkage upon curing, excellent thermal stability, and a low dielectric constant, they are highly valued [17–23]. A notable example is poly(BA-a), a benzoxazine resin synthesized from bisphenol A and
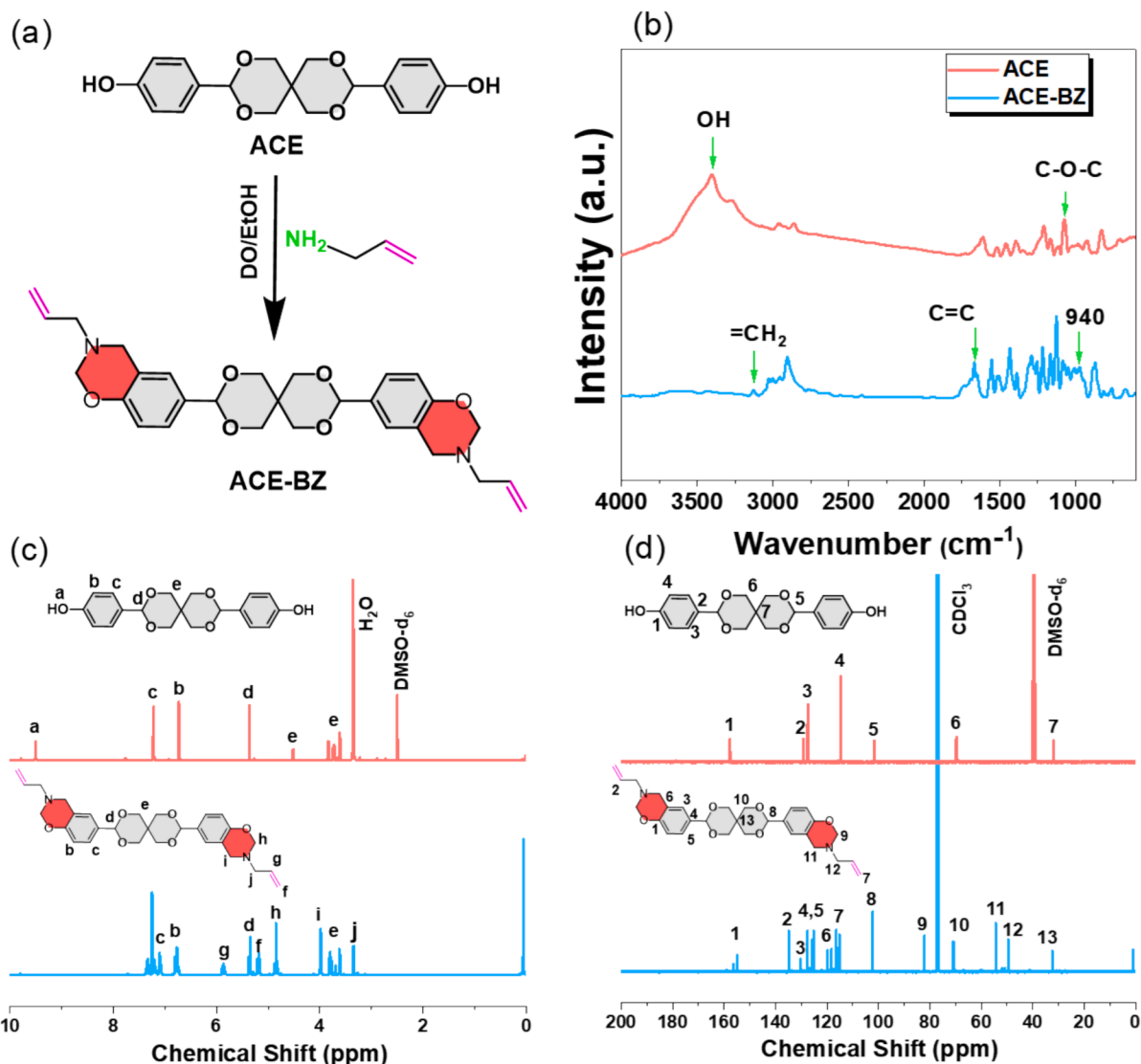
Fig. 1. (a) Synthesis of ACE-BZ monomer (b) FTIR, (c) ^{1}H NMR, and (d) ^{13}C NMR spectra of ACE and ACE-BZ.

aniline, which has been commercially utilized for over two decades in applications such as electronic packaging, aerospace, and transportation [24]. The versatility of macromolecular design in PBZs allows for the incorporation of various functionalities, significantly broadening their potential applications. Nevertheless, PBZs are not without limitations. For example, the ring-opening polymerization of benzoxazines requires elevated temperatures, and the resulting cured materials tend to be more brittle compared to other thermosetting materials, which restricts their use as matrices in certain high-performance composites. Additionally, at temperatures above 260 °C, the C–N–C bonds in non-crosslinked molecules are prone to cleavage, thereby constraining the high-temperature applicability of benzoxazine resins [25]. To address these challenges, the incorporation of organic functional groups [26–28], carbon-based materials [29,30], and silicon-based materials [31–33] into benzoxazine matrices has been explored. Such modifications can enhance the thermal and mechanical properties of the resins by promoting the formation of crosslinking networks and reducing chain mobility.

There has been a growing body of research focused on the potential advantages of incorporating polyhedral oligomeric silsesquioxane (POSS) nanoparticles (NPs) into polymer matrices. These nanoparticles have been shown to enhance thermal stability, reduce flammability, decrease density, lower thermal conductivity, increase oxidation resistance, and reduce surface free energy of the resulting composite materials [34–44]. The empirical chemical formula for POSS nanostructures is typically RSiO$_{1.5}$, where R denotes an organic group such as hydroxyl, acrylate, epoxy, arylene, or a hydrogen atom [45–48]. POSS nanoparticles can be incorporated into polymer matrices in various forms, either as mono-functional or multi-functional entities, resulting in POSS-polymer hybrids that can be classified into end-chain or side-chain variants, depending on the attachment point of the POSS moieties [49–53]. This approach has also been extended to BZ resins to develop polybenzoxazine nanocomposites with improved thermal stability and reduced brittleness [54–57]. Most previous studies have focused on blending low molecular weight BZ monomers with either monofunctional or octafunctional POSS macromers, followed by curing these mixtures at high temperatures to form organic–inorganic-based PBZs nanocomposites. For instance, Liu's group prepared PBZ containing double-decker silsesquioxane (DDSQ) and examined its thermal stability and ring-opening polymerization behavior [58]. Furthermore, our group developed a transparent and flexible PBZ by incorporating flexible polydimethylsiloxane (PDMS) and rigid DDSQ units. This resulted in a PDMS-BZ-DDSQ main chain-type PBZ copolymer following the thermal polymerization of the BZ monomer units [59]. In another study, our research group also synthesized a highly thermally stable and flexible PDMS-DABZ-DDSQ copolymer through a Diels–Alder reaction [17].
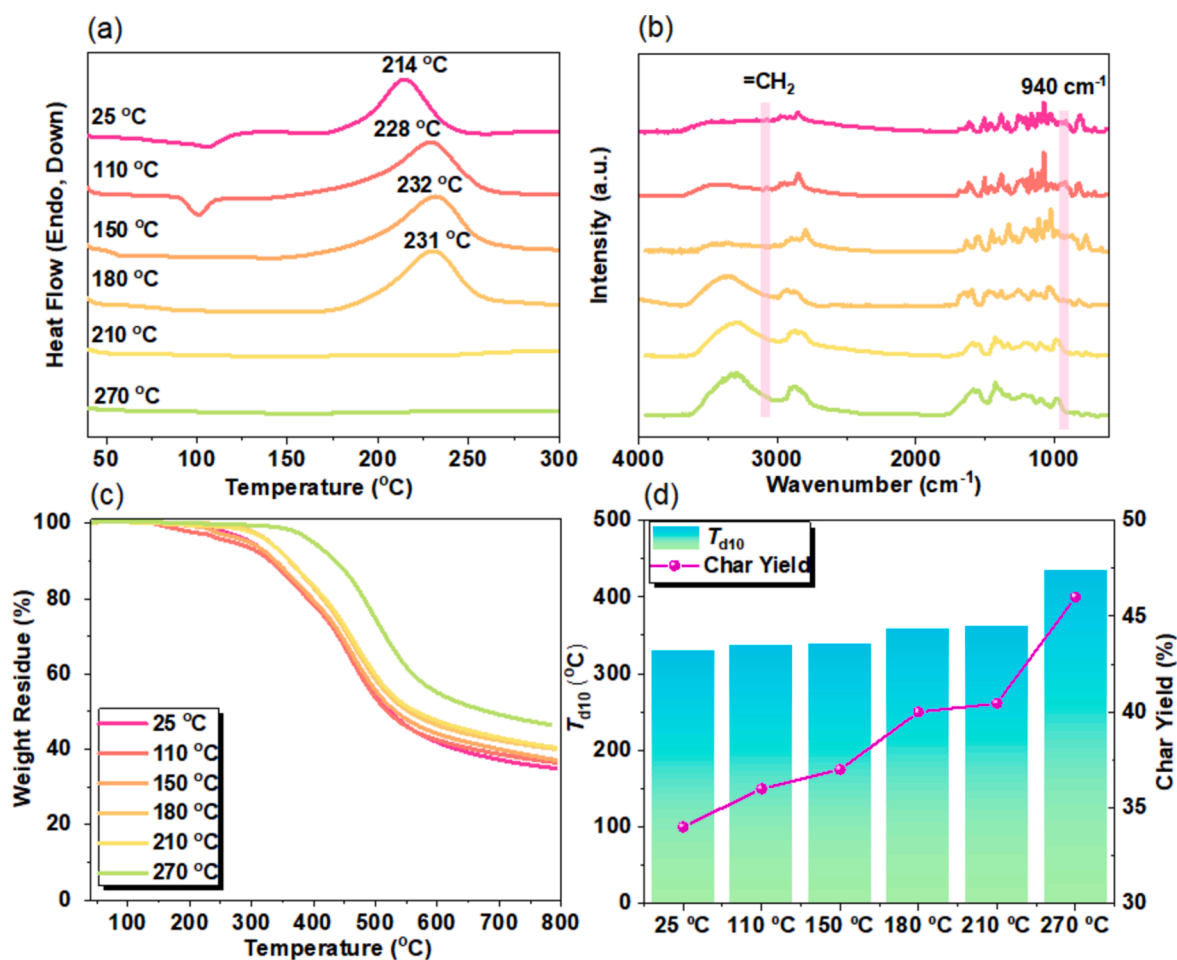
Fig. 2. (a) DSC, (b) FTIR spectra, (c) TGA analyses, and (d) char yield and T_{d10} values of ACE-BZ monomer before and after thermal polymerization at different temperatures.

High-performance polymers are essential for advanced applications due to their ability to withstand extreme temperatures without degradation, ensuring durability and reliability in fields such as aerospace, electronics, and automotive industries [17,59]. While extensive research has been conducted on diacetyl benzoxazines and POSS-functionalized benzoxazines as separate entities, limited studies have examined the combined effects of these materials. Diacetyl benzoxazines are known for their exceptional thermal stability and degradability [60], whereas POSS-benzoxazine nanocomposites exhibit superior mechanical and thermal properties, making them well-suited for high-performance applications [45]. However, to our knowledge, the potential synergistic effect of incorporating POSS into diacetyl-functionalized benzoxazines to achieve enhanced thermal stability remains unexplored.

In this study, we first synthesized an allyl-functionalized benzoxazine (BZ) with a rigid diacetal structure by reacting ACE with allylamine in the presence of paraformaldehyde, resulting in the formation of ACE-BZ. This novel compound was then subjected to further chemical modification through a hydrosilylation reaction with both DDSQ and POSS. The reaction with DDSQ yielded a main-chain DDSQ-ACE-BZ , while the reaction with POSS produced a highly crosslinked POSS-ACE-BZ. These DDSQ and POSS functionalized PBZ nanocomposites exhibited remarkable thermal stability and reduced activation energy compared to other PBZs materials, indicating their potential for high-performance applications. The primary objectives of this research were to explore the feasibility of incorporating POSS cages into PBZ matrices to create highly crosslinked networks and to investigate the effects of POSS on the thermal curing behavior, thermal stability, and activation energy of ACE-BZ crosslinked thermosets. Additionally, this

study aims to provide insights into how the integration of POSS and DDSQ into BZ structures can enhance the thermal properties of the resulting materials, thereby expanding their applicability in various advanced technological fields. The synthesized poly(DDSQ-ACE-BZ) and POSS-ACE-BZ exhibited outstanding thermal stability, with decomposition temperatures reaching 544 °C and 510 °C, respectively. This high-temperature resilience makes them well-suited for applications in industries such as electronics and automotive, where materials must withstand extreme thermal conditions.

2. Experimental section

2.1. Materials

Pentaerythritol, *p*-hydroxybenzaldehyde (*p*-BZCHO-OH), *p*-toluenesulfonic acid [PTSA], allylamine, sodium bicarbonate (Na₂CO₃), sodium hydroxide (NaOH), octakis(dimethylsilyloxy)octasilsesquioxane (ODMS-POSS), phenyltrimethylsilane, platinum divinyltetramethyldisiloxane complex [Pt(dvs)], and methyl dichlorosilane were purchased from Sigma-Aldrich. Petroleum ether (PE), N, N-dimethylformamide (DMF), 1,4-dioxane (DO), and toluene were supplied by obtained from Alfa Aesar. ACE was synthesized according to a previous study as shown in Scheme S1 [60]. The detailed synthesis procedures for double-decker silsesquioxane-Na (DD-Na) and DDSQ are included in the supporting information file.
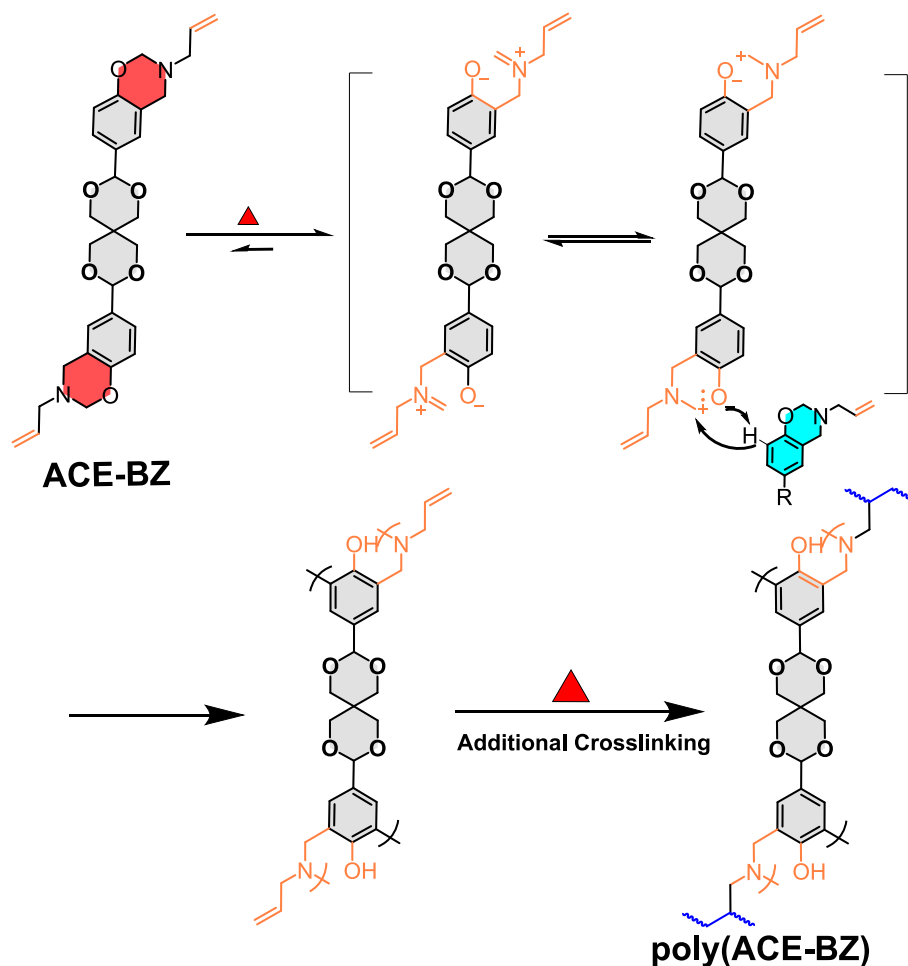
Fig. 3. Possible ring opening polymerization mechanism of ACE-BZ monomer to form poly(ACE-BZ).

2.2. Synthesis of ACE-BZ

A solvent system consisting of DO (60 mL) and EtOH (30 mL) was utilized to prepare a mixture containing ACE (1 g, 2.90 mmol), allylamine (0.33 mL, 7.53 mmol), and paraformaldehyde (0.39 g, 13 mmol). The reaction mixture was refluxed overnight at 100 °C while stirring. After the reaction was complete, the co-solvents were evaporated under reduced pressure, resulting in a white sticky liquid. To purify the crude product, it was diluted with EA and extracted with water and a 1 M NaOH solution. The organic phase was then dried over anhydrous Na_2SO_4, and the solvent was evaporated to yield a white solid product (yield: 94 %). FTIR (cm^{-1}): 2905 (aromatic CH), 1644 (C=C), and 940 (oxazine ring). ^1H NMR (DMSO-d_6, 500 MHz, δ, ppm): δ = 5.83, 5.36 (CH=CH$_2$), 4.82 (OCH$_2$N), 3.98 (ArCH$_2$N). ^{13}C NMR (DMSO-d_6, 125 MHz, δ, ppm): δ = 134.7, 116 (CH=CH$_2$), 82.04 (OCH$_2$N), 54.40 (ArCH$_2$N).

2.3. Synthesis of DDSQ-ACE-BZ and POSS-ACE-BZ

Toluene (100 mL) was added to a three-neck flask equipped with a reflux condenser, and DDSQ [17,59,61] ((0.5695 g, 0.49 mmol) and ACE-BZ (0.25 g, 0.49 mmol)), or ODMS-POSS (0.18 g, 0.176 mmol) and ACE-BZ (0.356 g, 0.704 mmol) and after adding 0.05 wt% of Pt(dvs), the reaction mixture was stirred and heated to 100 °C under reflux conditions in a nitrogen atmosphere. The reaction completion was observed by physical indicators like color change and most importantly by using thin-layer chromatography (TLC) to observe the reactants fully converted to desired compounds. Insoluble materials were removed from the mixture through filtration. The filtrate was then concentrated by vacuum distillation, resulting in the formation of a solid product. This solid was further dried in a vacuum oven to yield DDSQ-ACE-BZ (yield: 79 %) or POSS-ACE-BZ compound (yield: 85 %).

2.4. Thermal curing of ACE-BZ, DDSQ-ACE-BZ, and POSS-ACE-BZ

An aluminum pan containing the specified quantity of ACE-BZ, DDSQ-ACE-BZ, or POSS-ACE-BZ was heated in an oven from 110 to 270 °C at a rate of 5 °C/min for 2 h to afford poly(ACE-BZ), poly(DDSQ-ACE-BZ) and poly(POSS-ACE-BZ).

3. Results and discussion

3.1. Synthesis and characterization of ACE and ACE-BZ

The synthesis of ACE-BZ was achieved via a Mannich condensation reaction involving ACE, allylamine, and paraformaldehyde in a 2:1 mixture of DO and EtOH at 110 °C throughout 24 h [Fig. 1(a)]. The FTIR spectrum of ACE exhibited characteristic absorption bands at 3407, 1600–1500, and 1062 cm^{-1}, corresponding to the hydroxyl (OH) groups, aromatic vibrations, and C–O–C units of the diacetal structure, respectively [Fig. 1(b)]. Upon completion of the Mannich condensation to form ACE-BZ, the disappearance of the OH peak was noted, and new absorption bands appeared at 1670 and 940 cm^{-1}, indicative of the presence of C=C bonds and the oxazine ring, respectively [Fig. 1(b)]. The ^1H NMR spectrum of ACE-BZ [Fig. 1(c)] confirmed the disappearance of the OH signal from ACE. In addition, new signals were observed
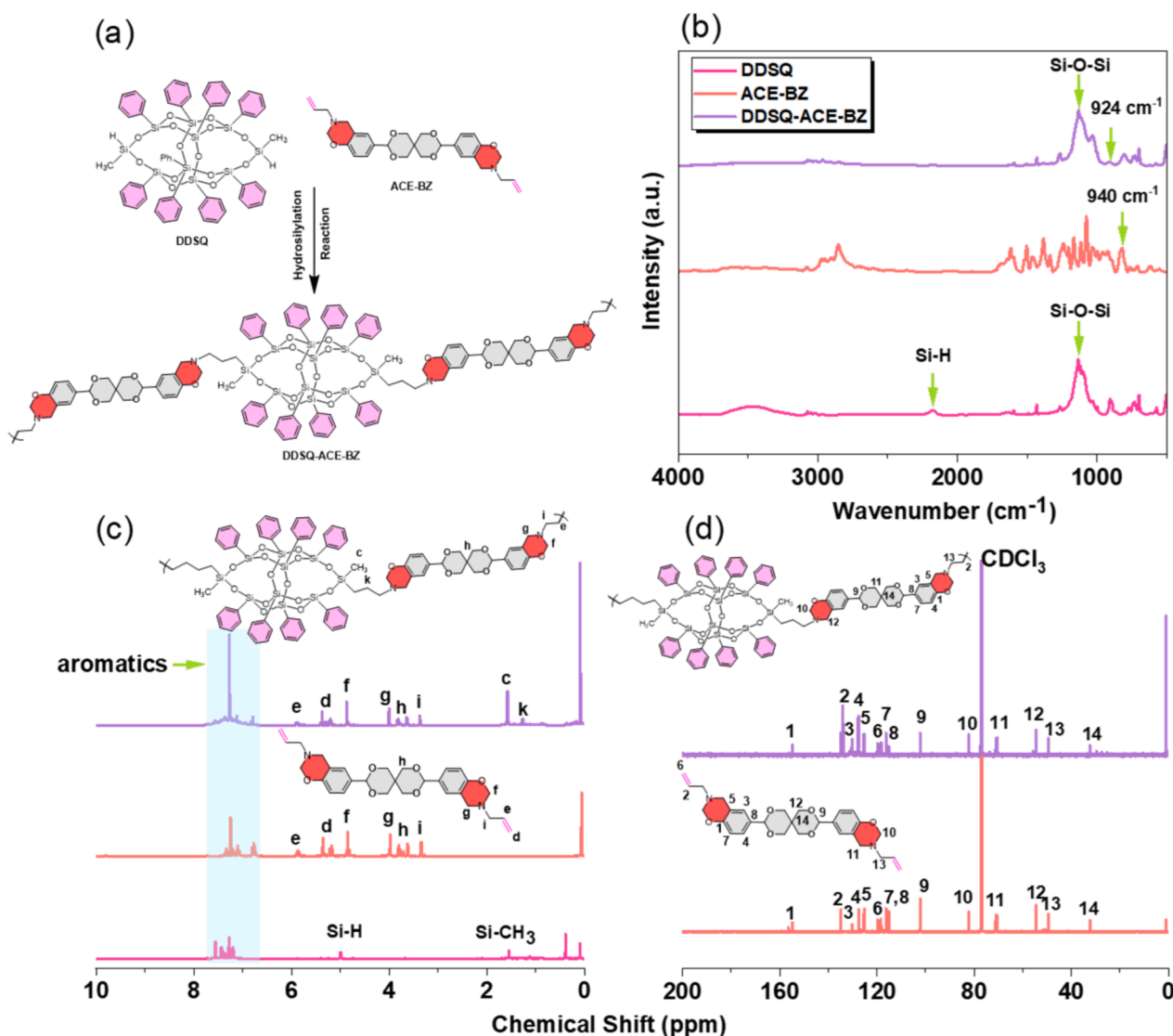
Fig. 4. (a) Synthesis of DDSQ-ACE-BZ, (b) FTIR, (c) ^{1}H NMR, spectra of DDSQ, ACE-BZ and DDSQ-ACE-BZ and (d) ^{13}C NMR spectra of ACE-BZ and DDSQ-ACE-BZ.

at 5.8 ppm and 5.3 ppm, corresponding to the CH$_2$=CH group derived from allylamine. The peaks at 4.8 ppm and 3.9 ppm were attributed to OCH$_2$N and ArCH$_2$N units, respectively, demonstrating that all hydroxyl groups in the ACE were involved in forming the oxazine ring. The remaining signals in the ACE-BZ spectrum originated from the ACE moiety, confirming the retention of a stable diacetal structure. Further structural verification was provided by the ^{13}C NMR spectrum of ACE-BZ, which displayed signals at 134.0 ppm (for =CH), 113.0 ppm (for =CH$_2$), 81.7 ppm (for OCH$_2$N), and 54.3 ppm (for ArCH$_2$N) [Fig. 1(d)]. Additionally, peaks at 32.23 ppm and 102.2 ppm were assigned to quaternary and tertiary carbon atoms within the diacetal framework, respectively. The lack of the OH signal and the clear presence of the oxazine ring unequivocally support the successful synthesis of the ACE-BZ monomer.

3.2. Thermal polymerization of ACE-BZ

The thermal ring-opening polymerization behavior of ACE-BZ monomer was systematically investigated using DSC, FTIR, and TGA [Fig. 2]. These analyses were performed over a temperature range from 25 °C to 270 °C. At 25 °C, the DSC thermogram displayed an endothermic peak at 105 °C and an exothermic peak at 214 °C, which indicates the high purity of the allyl-containing benzoxazine monomer

derived from ACE monomer [Fig. 2(a)]. Following thermal treatment at 110, 150, and 180 °C, the DSC curves exhibited thermal polymerization peaks at 228, 232, and 231 °C, respectively. However, after thermal treatment at temperatures of 210 °C and 270 °C, no further thermal polymerization peaks were observed, this suggests that the oxazine rings had fully undergone ROP at these temperatures [Fig. 2(a)]. In ACE-BZ, as the temperature rises, the exothermic peak shifts to higher values. Partial curing initiates around 110 °C, where cross-linking begins, creating a thermally stable network. This stabilized structure then requires a higher temperature to complete the ring-opening polymerization (ROP), leading to a shift in the exothermic peak. At elevated curing temperatures, specifically 210 °C and 270 °C, the absence of exothermic peaks indicates that the oxazine ring has fully undergone ROP, marking the completion of the curing process. The polymerization triggered by heat was further verified through FTIR spectroscopy [Fig. 2(b)]. As the thermal ROP temperature increased to 180 °C, the FTIR spectra revealed a new peak at 3350 cm^{-1}, indicating the presence of hydroxyl groups, along with a significant reduction in the intensity of the absorption band at 940 cm^{-1}, associated with the oxazine ring. Upon further heating beyond 210 °C, the characteristic peaks for the allyl group at 3090 cm^{-1} and the oxazine ring at 940 cm^{-1} disappeared completely, signifying the full ROP of the allyl groups and their additional reactivity at elevated temperatures, as shown in Fig. 2(b). These observations suggest that the
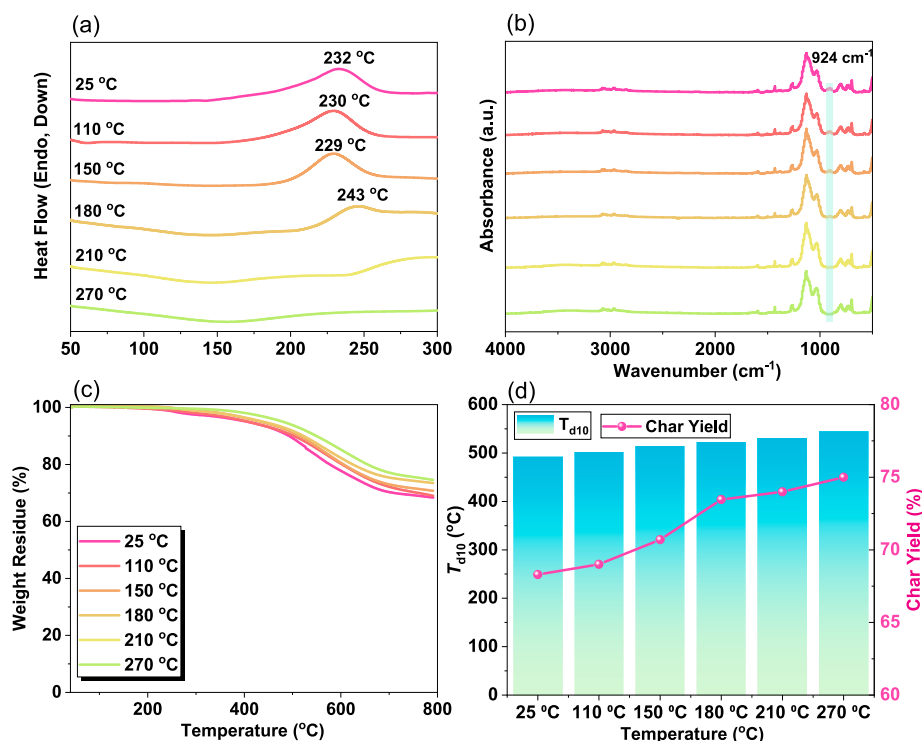
Fig. 5. (a) DSC, (b) FTIR spectra, (c) TGA analyses, and (d) char yield and T_{d10} values of DDSQ-ACE-BZ before and after thermal polymerization at different temperatures.
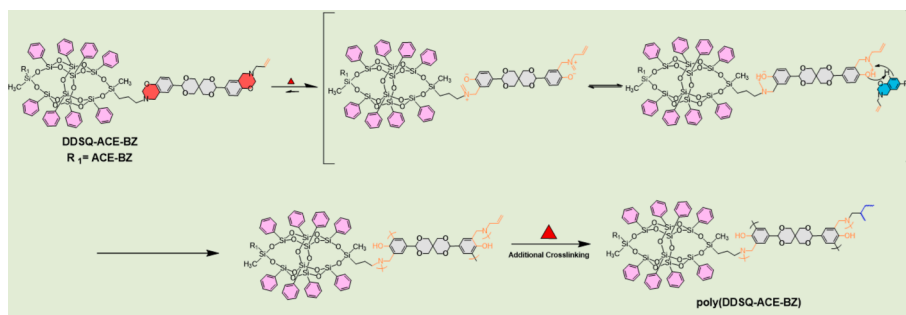

Fig. 6. Possible ring opening polymerization mechanism of DDSQ-ACE-BZ to form poly(DDSQ-ACE-BZ).

thermal polymerization of ACE-BZ involves two distinct reaction pathways. The primary pathway is the ROP of the oxazine ring, which occurs at relatively moderate temperatures. The secondary pathway involves an additional reaction of the allyl groups at higher temperatures, contributing to the overall polymerization process. This dual mechanism is crucial for understanding the thermal behavior and the stability of the resulting polymer networks formed from ACE-BZ [62]. Additionally, TGA was employed to assess the thermal stability of the ACE-BZ at various curing temperatures [Fig. 2(c)]. The degradation temperature (T_{d10}) and char yield at different curing conditions are presented in Fig. 2(d). For the uncured ACE-BZ, the T_{d10} was recorded at 330 °C with a char yield of 34 wt%. Upon curing at 270 °C, the thermal stability significantly improved, with T_{d10} increasing to 435 °C and the char yield reaching 46 wt%.

The improvement in thermal stability is attributable primarily to the ROP of the oxazine rings and the additional polymerization of the allyl groups, which together promote the formation of a highly cross-linked poly(ACE-BZ) network with reduced moisture content at elevated temperatures [Fig. 3] [63]. Furthermore, the significant intra- and intermolecular hydrogen bonding (OH···O) that develops during the ROP process plays a crucial role in enhancing the thermal stability of the PBZ

[64]. Collectively, these components contribute to the robust thermal performance of the thermal-cured ACE-BZ, making it a promising material for high-temperature applications. The proposed polymerization mechanism of the ACE-BZ is illustrated in Fig. 3. At high temperatures, the O–C bond in the Ar–O–CH$_2$ structure breaks, generating a carbocation (C$^+$) and an oxygen anion (O$^-$). This reaction likely triggers the thermal ring-opening of the oxazine ring in ACE-BZ. Following this, the N–CH$^+$ group attaches to the *ortho*-position on an adjacent ring, forming a Mannich bridge. Meanwhile, the O$^-$ abstracts a hydrogen from the *ortho*-position of a neighboring ring, resulting in the formation of a phenolic OH group.

3.3. Synthesis, characterization, and ROP behavior of the DDSQ-ACE-BZ

In DDSQ-ACE-BZ synthesis, both DDSQ and ACE-BZ contain bifunctional reactive sites, so we selected a 1:1 ratio to produce a linear DDSQ-ACE-BZ polymer with a main chain structure. Fig. 4(a) illustrates the synthesis of the main-chain DDSQ-ACE-BZ via a hydrosilylation reaction between DDSQ and ACE-BZ. The existence of the oxazine ring in DDSQ-ACE-BZ was confirmed using FTIR and NMR spectroscopy. The FTIR spectrum of DDSQ displayed characteristic absorption bands at
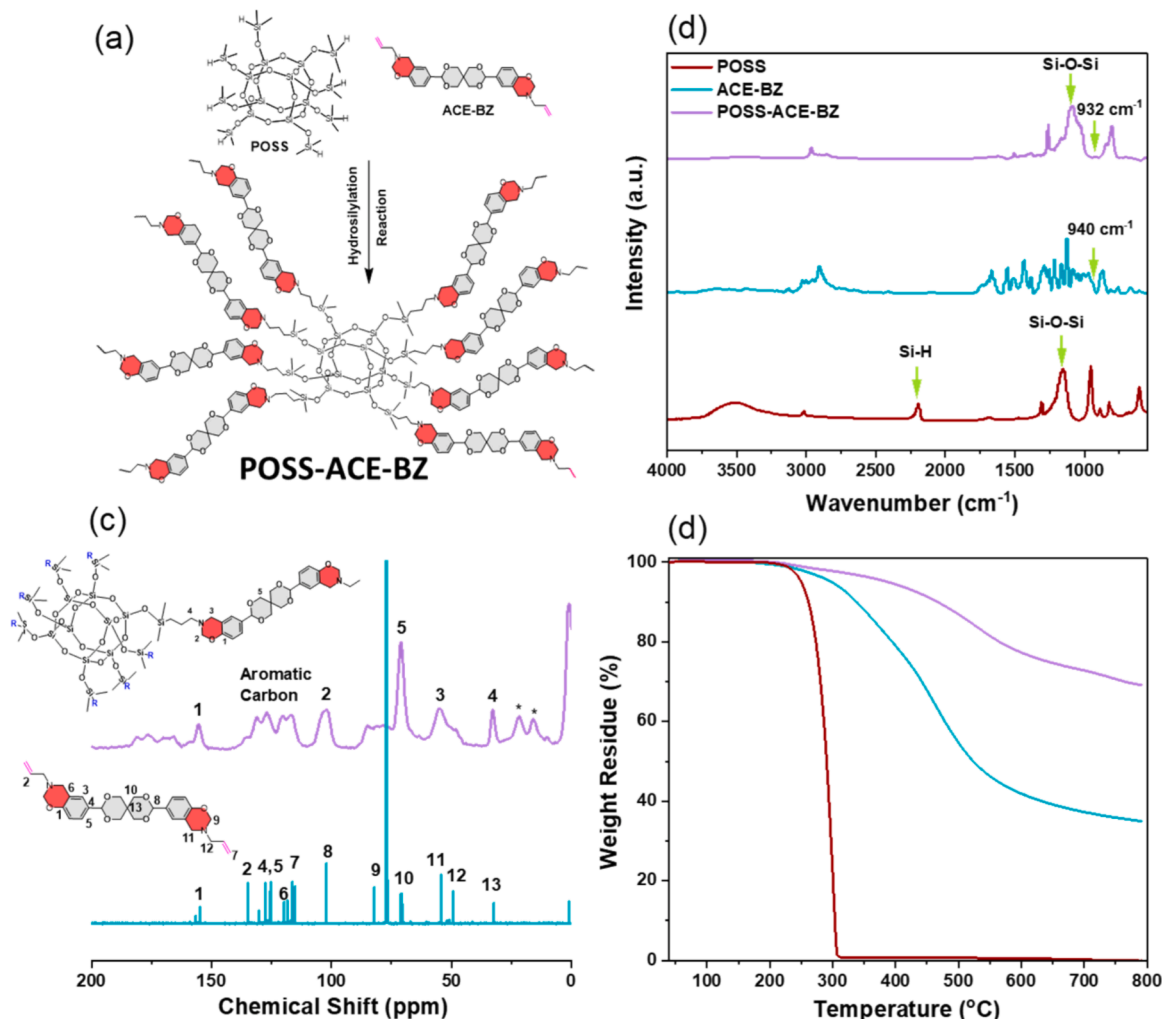
Fig. 7. (a) Synthesis of POSS-ACE-BZ (b) FTIR profiles of POSS, ACE-BZ and POSS-ACE-BZ, (c) ^{13}C NMR and SS ^{13}C NMR spectra of ACE-BZ and POSS-ACE-BZ. (d) TGA spectra of POSS, ACE-BZ and POSS-ACE-BZ.

2175 cm^{-1} and 1122 cm^{-1}, corresponding to the Si–H and Si–O–Si groups, respectively. After the hydrosilylation reaction, the disappearance of the Si–H peak in the DDSQ-ACE-BZ spectrum, along with the appearance of a new band at 924 cm^{-1} indicatives of the oxazine ring, confirmed the successful reaction [Fig. 4(b)]. This observation was further corroborated by the ^{1}H NMR spectrum of DDSQ-ACE-BZ, where the signal for the Si–H group at 4.99 ppm, present in DDSQ, was completely absent, validating the complete hydrosilylation process. Additionally, two distinct signals at 4.89 ppm and 3.98 ppm, corresponding to the OCH$_2$N and ArCH$_2$N units of the oxazine ring, were observed in the DDSQ-ACE-BZ spectrum [Fig. 4(c)]. The presence of terminal double bonds in the main chain of DDSQ-ACE-BZ was evidenced by signals at 5.3 ppm and 4.8 ppm in the ^{1}H NMR spectrum, which align with those from the terminal double bonds of ACE-BZ. Furthermore, additional proton signals corresponding to the quaternary and tertiary carbon atoms of the diacetal framework were also detected, indicating that the diacetal structure of ACE-BZ remained. The ^{13}C NMR spectrum of DDSQ-ACE-BZ further supported these findings, displaying signals characteristic of the oxazine ring at 82 ppm and 55 ppm, as well as signals for the terminal double bonds at 134 ppm and 113 ppm, respectively [Fig. 4(d)]. These results collectively confirm the successful synthesis and structural integrity of the DDSQ-ACE-BZ compound following hydrosilylation.

To study the ROP of DDSQ-ACE-BZ, TGA, DSC, and FTIR spectroscopy were employed at various temperatures [Fig. 5]. At ambient temperature, the DSC traces of the DDSQ-ACE-BZ exhibited a distinct exothermic curing peak at 232 °C [Fig. 5(a)], indicative of high purity. This peak signifies the formation of poly(DDSQ-ACE-BZ) at elevated temperatures, resulting from thermal activation and subsequent ring-opening of the oxazine ring in DDSQ-ACE-BZ. After additional thermal treatment at 110 and 180 °C, the exothermic peaks shifted slightly to 230, 229, and 243 °C, respectively. The decreasing intensity of these curing peaks suggests the presence of an underlying catalytic effect. However, when the thermal treatment temperature was raised to 210 and 270 °C, the exothermic peak completely disappeared [Fig. 5(a)], indicating that the curing process was fully completed. To elucidate the structural changes occurring in DDSQ-ACE-BZ during thermal curing, in situ FTIR spectroscopy was conducted at various temperatures [Fig. 5 (b)]. The distinctive absorption bands of DDSQ-ACE-BZ at 934 cm^{-1} attributed to the oxazine ring as the curing temperature rose from 110 to 180 °C, and remained observable, though with diminishing intensities. Upon further heating to 210 and 270 °C, these peaks were no longer detected, signifying the completion of ROP of the oxazine rings, resulting in a cross-linked and highly thermally stable poly(DDSQ-ACE-BZ). To assess the thermal stability of DDSQ-ACE-BZ, TGA measurements were performed to determine the degradation temperature at 10 % weight loss and the char yield. These parameters were evaluated before and after the thermal curing of DDSQ-ACE-BZ at different temperatures [Fig. 5(c) and 5(d)]. The T_{d10} and char yield for uncured DDSQ-ACE-BZ were found to be 492 °C and 69 wt%, respectively. Following curing at
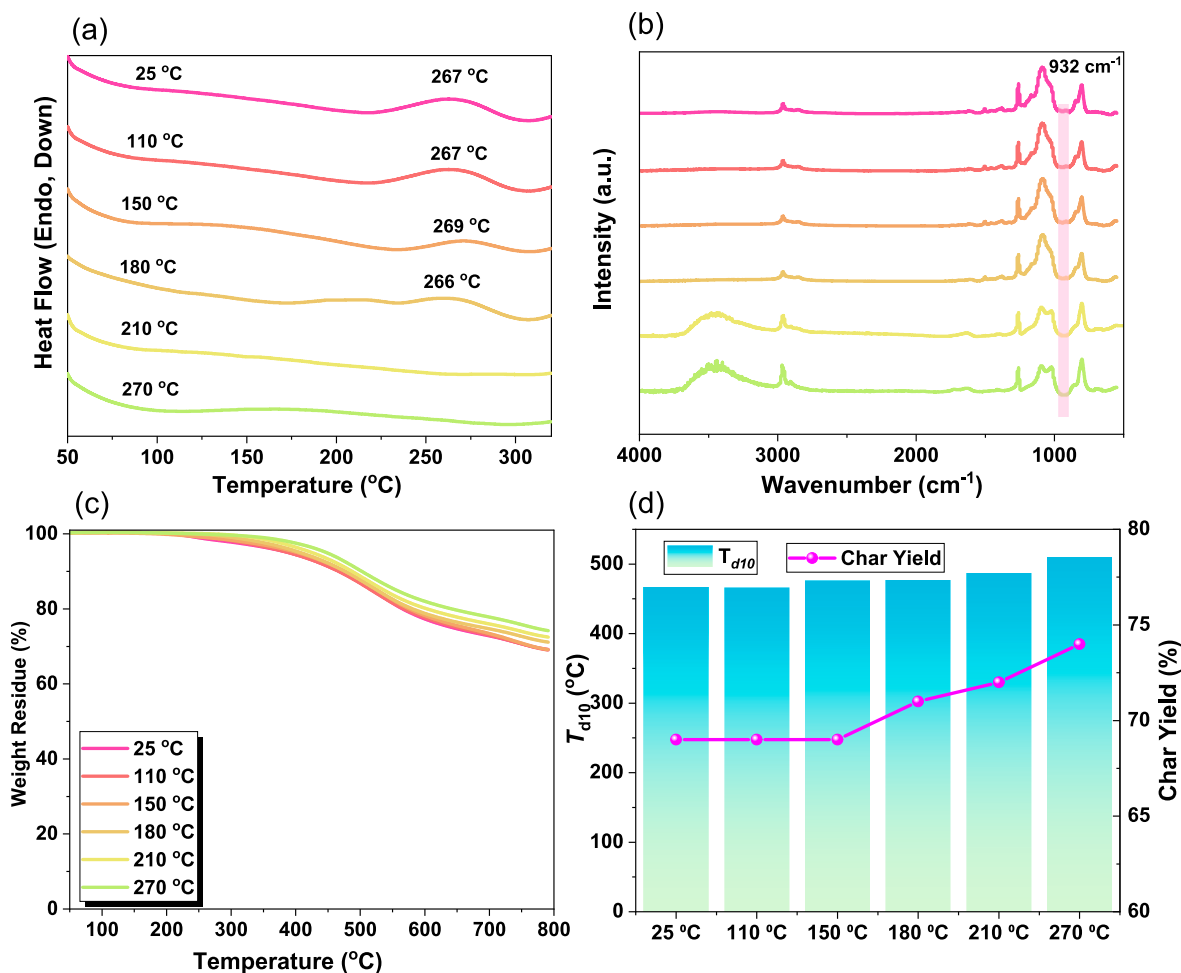
Fig. 8. (a) DSC, (b) FTIR spectra, (c) TGA analyses, (d) char yield and T_{d10} values of POSS-ACE-BZ before and after thermal polymerization at different temperatures.

150, 180, 210, and 270 °C, the T_{d10} values increased progressively to 502, 514, 522, 531, and 544 °C, respectively.

The reason for this improvement in thermal stability is the robust rigid DDSQ units in the DDSQ-ACE-BZ structure and the ROP of the oxazine groups, which contributes to the formation of a more crosslinked and stable polymer network with a superior thermal resistance [Fig. 6] [65]. Fig. 6 shows the possible ROP mechanism of the DDSQ-ACE-BZ to form poly(DDSQ-ACE-BZ) [65].

3.4. Preparation, characterization, and ROP behavior of the POSS-ACE-BZ

In the case of POSS-ACE-BZ, we combined an 8-functional monomer (POSS) with a bifunctional monomer (ACE-BZ) in a 1:4 ratio. Each POSS molecule, having eight reactive sites, can potentially bind with up to eight bifunctional ACE-BZ molecules. The 1:4 ratio ensures an ample supply of bifunctional monomers, allowing multiple crosslinking points per multifunctional monomer, effectively "linking" several chains together. This results in a densely interlinked network. The crosslinked POSS-ACE-BZ networks were also synthesized via a hydrosilylation reaction involving ACE-BZ and POSS monomers, as depicted in Fig. 7(a). The successful occurrence of the hydrosilylation reaction and the presence of the BZ ring was confirmed using spectroscopy analyses including NMR and FTIR. In the FTIR pattern of POSS [Fig. 7(b)], Typical signals were seen at 2203 and 1153 cm^{-1}, according to the Si–H and Si–O–Si groups, respectively. After hydrosilylation, the Si–H peak in the POSS-ACE-BZ spectra disappeared, and a band at 932 cm^{-1} appeared, indicating the presence of the oxazine ring and the formation of POSS-ACE-

BZ. Additionally, the Si–O–Si peak of POSS-ACE-BZ was broadened compared to that of POSS, suggesting the formation of a crosslinked structure [66,67]. Due to the insolubility of POSS-ACE-BZ in organic solvents, solid-state ^{13}C NMR was employed to further characterize POSS-ACE-BZ. Aromatic carbon signals were detected between 115–131 ppm, and two oxazine ring proton signals were observed at 82 and 55 ppm, representing the OCH$_2$N and ArCH$_2$N units, respectively [Fig. 7(c)]. Furthermore, TGA was used to assess the thermal stability of POSS-ACE-BZ [Fig. 7(d)]. The T_{d10} and char yield values of POSS and ACE-BZ were found to be 261 °C with 0 wt% and 338 °C with 35 wt%, respectively. After the hydrosilylation reaction, the T_{d10} and char yield values of POSS-ACE-BZ increased substantially to 467 °C and 68 wt%, respectively, indicating enhanced thermal stability due to the crosslinking of POSS and ACE-BZ.

The thermal polymerization behavior of POSS-ACE-BZ was further investigated using DSC and FTIR at various stages of heat treatment, as shown in Fig. 8(a) and (b). The DSC analysis of the POSS-ACE-BZ revealed thermal curing peaks at 267, 269, and 266 °C as the heat treatment temperature was incrementally increased from 100 to 180 °C [Fig. 8(a)]. Fig. 8(a) illustrates the disappearance of the oxazine peak after thermal treatment between 210 and 270 °C. The DDSQ and POSS exhibit exceptional thermal stability due to their inorganic, cage-like rigid structures. When incorporated into the ACE-BZ monomer, they form a highly crosslinked, rigid framework that increases chain stiffness. This added rigidity restricts chain mobility, requiring greater thermal energy to enable necessary rearrangements and crosslinking, thus shifting the exothermic peak to higher temperatures. Concurrently, Fig. 8(b) shows a progressive decrease and eventual disappearance of
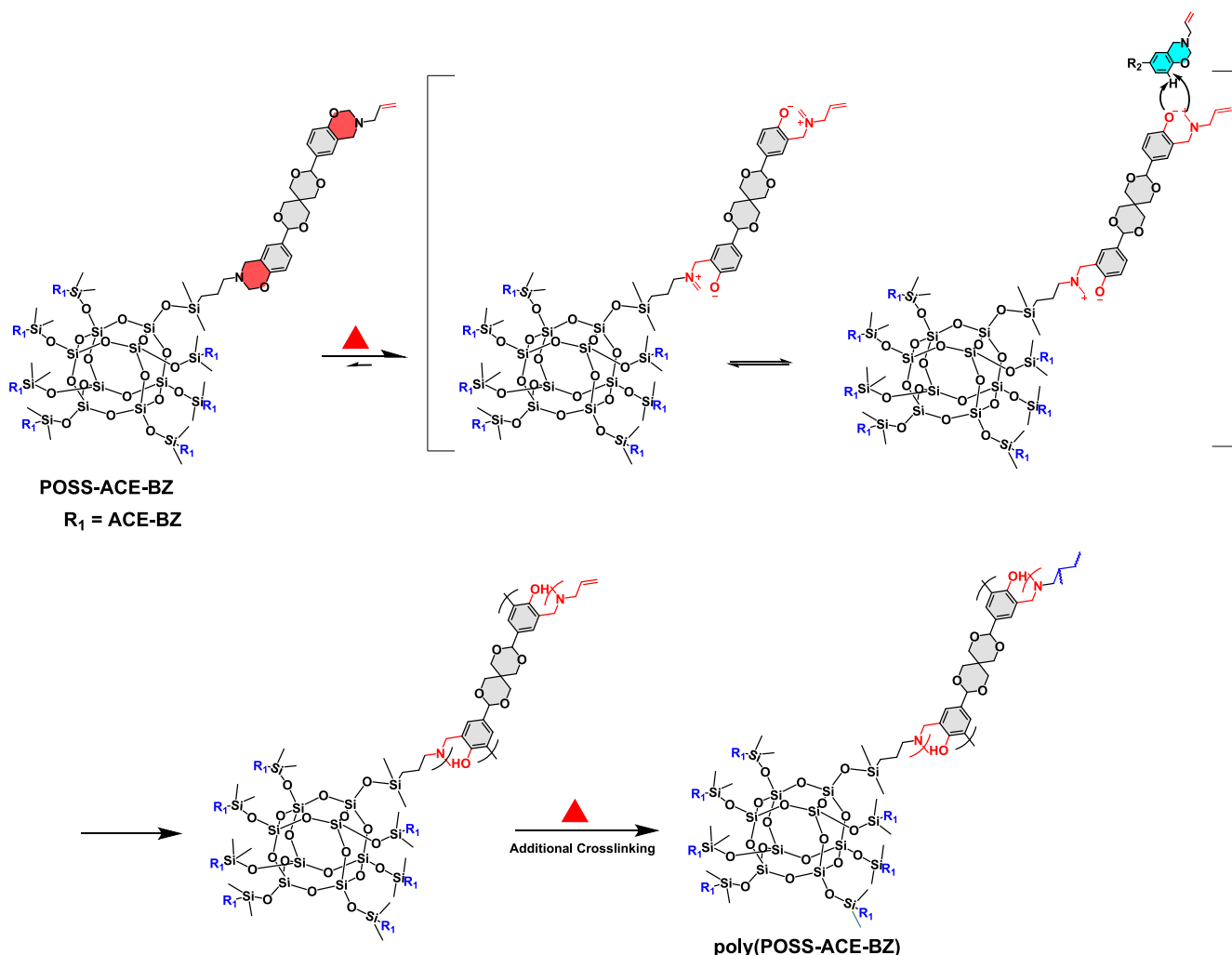
Fig. 9. Possible ring opening polymerization mechanism of POSS-ACE-BZ to form poly(POSS-ACE-BZ).

the BZ ring's absorption bands at 932 cm^{-1} as the curing temperature was raised from 100 to 180 °C, vanishing completely at 210 and 270 °C. These observations are consistent with the DSC results depicted in Fig. 8 (a). Furthermore, TGA analysis of the uncured POSS-ACE-BZ, as shown in Fig. 8(c), indicated a T_{d10} value of 467 °C and a char yield of 69 wt%. After sequential heat treatments, the Td10 values recorded were 466, 476, 477, 487, and 510 °C, with corresponding char yields of 69, 70, 71, 72, and 74 wt%, respectively, as illustrated in Fig. 8(c) and (d).

Fig. 9 illustrates the formation of poly(POSS-ACE-BZ) with a highly crosslinked three-dimensional network structure [65]. This structure includes additional crosslinking provided by C═C groups [68]. The insolubility of POSS-ACE-BZ polymers significantly influences both their processing and applications. This property offers notable advantages in terms of durability, as insoluble materials typically exhibit enhanced chemical resistance, making POSS-ACE-BZ polymers well-suited for protective coatings and membranes exposed to high pH or corrosive environments [32,50]. Additionally, their high thermal stability renders them suitable for demanding applications in electronics, automotive, and aerospace industries, where materials are required to function as thermally stable adhesives or insulating layers [39]. The morphology of DDSQ-ACE-BZ and POSS-ACE-BZ was analyzed using SEM, and the presence of heteroatoms was further verified through SEM elemental mapping, as shown in Fig. S1. SEM images revealed an irregular and disordered spherical morphology for both DDSQ-ACE-BZ and POSS-ACE-BZ [Fig. S1(a) and (b)], indicating a non-uniform structure at the microscale. The observed irregular morphology suggests an increase in

surface roughness, which may significantly impact various applications. In adhesive and coating technologies, enhanced surface roughness often promotes improved mechanical interlocking and stronger substrate adhesion [32,50]. Additionally, in optical and photonic applications, irregular morphologies can contribute to light scattering, rendering them useful for anti-reflective coatings and optical diffusers [39]. Consequently, this surface roughness expands the potential applicability of DDSQ-ACE-BZ and POSS-ACE-BZ across diverse technical fields. SEM elemental mapping [Fig. S1(c–j)] confirmed the distribution of C (red color), N (blue color), O (green color), and Si (white color) throughout the samples. This elemental analysis supports the presence of the oxazine ring, and the rigid silicon framework associated with DDSQ and POSS, highlighting the successful incorporation of these components into the polymer matrices.

3.5. DSC kinetics of ACE-BZ, DDSQ-ACE-BZ and POSS-ACE-BZ

We investigated the activation energy (E_a) of ACE-BZ, DDSQ-ACE-BZ, and POSS-ACE-BZ using DSC analysis at varying heating rates [5, 10, 15, and 20 °C min^{-1}], as shown in Fig. 10. The E_a values were calculated using the Kissinger and Ozawa methods. Based on the Kissinger analysis, the E_a values for ACE-BZ, DDSQ-ACE-BZ, and POSS-ACE-BZ were determined to be 95.89, 117.17, and 162 kJ/mol, respectively. The Ozawa method yielded E_a values of 104.2, 127.47, and 164.5 kJ/mol for ACE-BZ, DDSQ-ACE-BZ, and POSS-ACE-BZ, respectively. The order of E_a values was found to be POSS-ACE-BZ > DDSQ-ACE-BZ > ACE-BZ. The
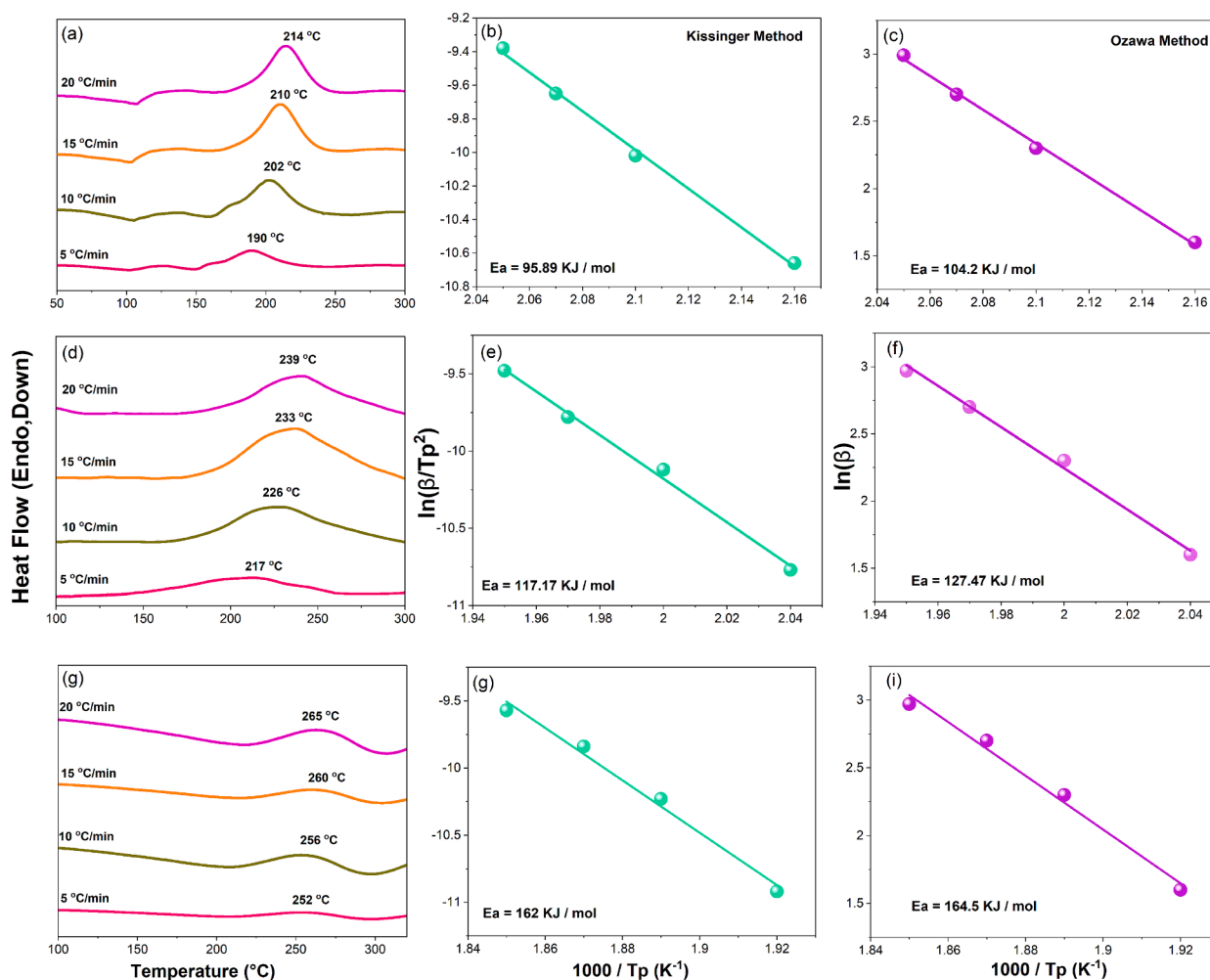
Fig. 10. DSC kinetics at different heating rates and their activation energy values (a–c) ACE-BZ monomer, (d–f) DDSQ-ACE-BZ, and (g–i) POSS-ACE-BZ.

ACE-BZ monomer, being a small molecule with high mobility, requires relatively low energy to initiate the ROP of the oxazine unit compared to DDSQ-ACE-BZ and POSS-ACE-BZ. The highly crosslinked POSS-ACE-BZ is composed of ACE-BZ units interconnected by covalent bonds, forming a three-dimensional network. Consequently, the ROP of the oxazine units in POSS-ACE-BZ is more difficult, resulting in higher activation energy for POSS-ACE-BZ [69].

3.6. Comparison of ROP behavior and thermal properties of ACE-BZ, DDSQ-ACE-BZ, and POSS-ACE-BZ

Fig. 11 presents a comparison of the DSC curves and thermal stability of ACE-BZ, DDSQ-ACE-BZ, and POSS-ACE-BZ. The exothermic curing peak for ACE-BZ was observed at 214 °C, which increased to 232 °C for DDSQ-ACE-BZ and 267 °C for POSS-ACE-BZ after the hydrosilylation reaction between ACE-BZ with DDSQ and POSS, respectively [Fig. 11 (a)]. This increase in curing temperatures of the DDSQ-ACE-BZ and POSS-ACE-BZ can be attributed to the rigid structures of DDSQ and POSS. T_{d10} and char yield for ACE-BZ, DDSQ-ACE-BZ, and POSS-ACE-BZ were measured as 338 °C with a 35 wt% char yield, 492 °C with a 69 wt% char yield, and 467 °C with a 68 wt% char yield, respectively [Fig. 11 (b) and (c)]. After the ROP process at 270 °C, the T_{d10} and char yield for poly(ACE-BZ), poly(DDSQ-ACE-BZ), and poly(POSS-ACE-BZ) increased to 435 °C with a 46 wt% char yield, 544 °C with a 75 wt% char yield, and 510 °C with a 74 wt% char yield, respectively [Fig. 11(d) and (e)]. Notably, our poly(DDSQ-ACE-BZ), and poly(POSS-ACE-BZ) exhibit higher T_{d10} values than previously reported thermally stable

polybenzoxazines, indicating superior thermal stability due to the rigid structures of DDSQ and POSS [Fig. 11(f) and Table S1]. To gain deeper insight into the thermal degradation behavior of these PBZ materials, derivative weight loss curves were analyzed, as shown in Fig. S2. The derivative weight loss curve of ACE-BZ exhibited three distinct decomposition stages: the first peak, between 210–230 °C, corresponds to the ROP of the oxazine ring, the second peak, at 330–350 °C, indicates the breakdown of diacetal groups; and the final peak signifies the complete decomposition of the ACE-BZ monomer [Fig. S2(a)]. In comparison, DDSQ-ACE-BZ and POSS-ACE-BZ displayed a complete degradation peak at 500–550 °C [Fig. S2(a)]. After ROP at 270 °C, the thermal degradation temperatures of poly(ACE-BZ), poly(DDSQ-ACE-BZ), and poly(POSS-ACE-BZ) increased, consistent with TGA analysis [Fig. S2 (b)]. The higher thermal stability of DDSQ-ACE-BZ compared to POSS-ACE-BZ is primarily due to the greater thermal stability of the DDSQ molecule with eight aromatic rings compared to POSS with sixteen CH$_3$ units [17].

4. Conclusion

The incorporation of DDSQ and POSS units into the polybenzoxazine matrix significantly enhanced the thermal properties of the resulting nanocomposites. The hydrosilylation reaction provided a robust synthetic route, enabling the effective integration of these nanostructures within the polymer backbone. Comprehensive characterization using NMR and FTIR spectrometry confirmed the successful synthesis of the desired DDSQ and POSS functionalized PBZ. Remarkably, after thermal
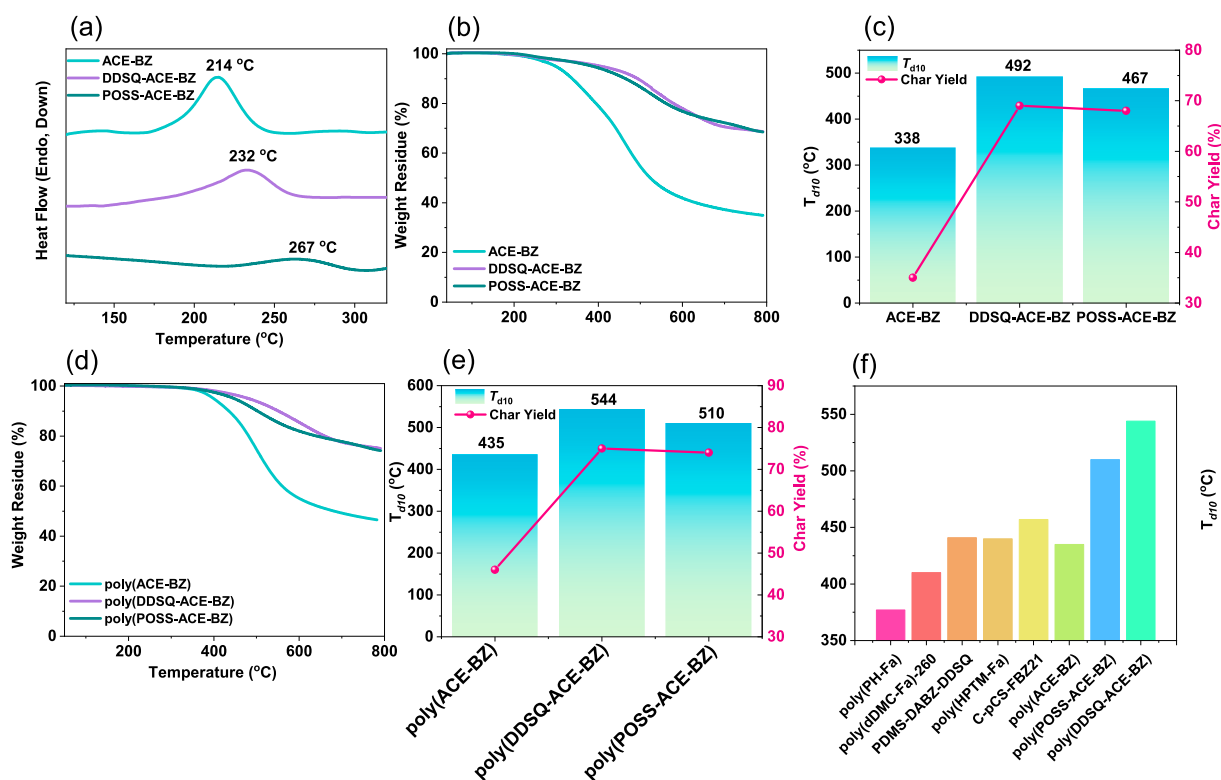
Fig. 11. Comparison of (a) DSC (b) TGA, (c) T_{d10}, and char yield (wt%) of ACE-BZ, DDSQ-ACE-BZ, and POSS-ACE-BZ. (d) and (e) Comparison of thermal stability of poly(ACE-BZ), poly(DDSQ-ACE-BZ), and poly(POSS-ACE-BZ), (f) Comparison of thermal stability (T_{d10}) poly(ACE-BZ), poly(DDSQ-ACE-BZ) and poly(POSS-ACE-BZ) with other PBZs precursors.

curing at 270 °C, the DDSQ-ACE-BZ nanocomposite exhibited a T_{d10} of 544 °C and a char yield of 75 wt%, while the POSS-ACE-BZ nanocomposite achieved a T_{d10} of 510 °C and a char yield of 74 wt%. High-temperature polymers are critical in aerospace, electronics, and automotive industries due to their durability under extreme thermal conditions. The synthesized poly(DDSQ-ACE-BZ) and poly(POSS-ACE-BZ) demonstrate exceptional thermal stability, withstanding temperatures of up to 544 °C and 510 °C, respectively, making them highly suitable for high-temperature applications. These remarkable thermal properties highlight the potential of DDSQ and POSS-functionalized polybenzoxazines for advanced applications demanding materials capable of enduring extreme thermal environments. This development represents a significant advancement in high-performance polymer nanocomposites, setting a new benchmark for thermal stability in the field.

CRediT authorship contribution statement

Mohsin Ejaz: Writing – original draft, Methodology, Investigation. **Mohamed Gamal Mohamed:** Writing – review & editing, Writing – original draft, Supervision, Methodology, Formal analysis, Data curation, Conceptualization. **Wei-Chun Huang:** Investigation, Formal analysis. **Yang-Chin Kao:** Formal analysis, Conceptualization. **Wei-Cheng Chen:** Data curation. **Shiao-Wei Kuo:** Supervision, Project administration, Funding acquisition.

Declaration of competing interest

The authors declare that they have no known competing financial interests or personal relationships that could have appeared to influence the work reported in this paper.

Appendix A. Supplementary data

Supplementary data to this article can be found online at https://doi.org/10.1016/j.eurpolymj.2024.113649.

Data availability

The data that has been used is confidential.

References

[1] K. Kong, J. Gargiuli, K. Kanari, M.Y. Rivera Lopez, J. Thomas, G. Worden, L. Lu, S. Cooper, S. Donovan-Holmes, A. Mathers, N. Hewlings, A. Suliga, J. Wessing, S. Vincent-Bonnieu, K. Robson Brown, I. Hamerton, Physical and mechanical properties of nano-modified polybenzoxazine nanocomposite laminates: pre-flight tests before exposure to low Earth orbit, Compos. Part B 276 (2024) 111311, https://doi.org/10.1016/j.compositesb.2024.111311.
[2] M.S. Selim, S.A. El-Safty, M.A. Shenashen, A. Elmarakbi, Advances in polymer/inorganic nanocomposite fabrics for lightweight and high-strength armor and ballistic-proof materials, Chem. Eng. J. 493 (2024) 152422, https://doi.org/10.1016/j.cej.2024.152422.
[3] Y. Zhang, X. Liu, R. Yang, Q. Zhuang, Lightweight polybenzoxazole aerogels with high compressive strength, ultralow dielectric constants, and excellent thermal stability, Polym. Chem. 15 (9) (2024) 924–936, https://doi.org/10.1039/D3PY01325A.
[4] X.K. Li, A.P. Zhang, J. Bian, K.Y. Ni, W. Zhao, K.C. Yang, H.L. Lin, D.Q. Chen, Progress on the simulation, synthesis, processing and application of high performance thermosetting polybenzoxazine resin and its composites: a review, Prog. Org. Coat. 192 (2024) 108506, https://doi.org/10.1016/j.porgcoat.2024.108506.

[5] Y.-Y. Xie, W.-T. Yang, G. Wu, S.-C. Chen, Y.-Z. Wang, Defect engineering for upcycling commodity thermosetting polymers to multifunctional carbon sponges toward multi-scenario applications, Carbon 229 (2024) 119478, https://doi.org/10.1016/j.carbon.2024.119478.

[6] Y. Shen, S. Wang, G. Du, T. Qin, S. Jiang, S. Liu, Z. Duan, H. Niu, T. Li, Laminated composite fabricated using high-performance polyamine thermoset: ultra heat resistance and excellent mechanical property, Compos. B 272 (2024) 111209, https://doi.org/10.1016/j.compositesb.2024.111209.

[7] H. Wang, T. Li, J. Li, R. Zhao, A. Ding, F.-J. Xu, Structural engineering of polyurethanes for biomedical applications, Prog. Polym. Sci. 151 (2024) 101803, https://doi.org/10.1016/j.progpolymsci.2024.101803.

[8] J. Jiang, X. Tao, T. Yang, D. Chen, C. Yin, S. Xing, J. Tang, Synergistic improvements in the processability and mechanical properties of cyanate esters via aminobenzonitrile-induced chemical tailoring, J. Mater. Chem. A 12 (2024) 21944–21955, https://doi.org/10.1016/10.1039/D4TA02460E.

[9] L. Liu, Y. Duan, H. Yun, X. Chen, J. Liu, S. Lv, Y. Zhang, Progress on the research and development of the biomass-based polyimide, Ind. Crops Prod. 220 (2024) 119239, https://doi.org/10.1016/j.indcrop.2024.119239.

[10] M.B. Whittaker, J.P. Foreman, Identifying the influences on network formation in structural isomers of multifunctional epoxies using near-infrared spectroscopy, Macromolecules 57 (2024) 3438–3450, https://doi.org/10.1021/acs.macromol.4c00274.

[11] Y.-C. Kao, M.G. Mohamed, C.-H. Chiang, S.-W. Kuo, Design and construction of furan-based and thiophene-based salicyladazine bisbenzoxazine resins with high thermal stability and tunable surface properties, Macromol. Chem. Phys. (2024) 2400091, https://doi.org/10.1002/macp.202400091.

[12] M. Ejaz, M.G. Mohamed, Y.-T. Chen, K. Zhang, S.-W. Kuo, Porous carbon materials augmented with heteroatoms derived from hyperbranched biobased benzoxazine resins for enhanced CO_2 adsorption and exceptional supercapacitor performance, J. Energy Storage 78 (2024) 110166, https://doi.org/10.1016/j.est.2023.110166.

[13] M.G. Mohamed, C.-C. Chen, K. Zhang, S.-W. Kuo, Construction of three-dimensional porous organic polymers with enhanced CO_2 uptake performance via solid-state thermal conversion from tetrahedral benzoxazine-linked precursor, Eur. Polym. J. 200 (2023) 112551, https://doi.org/10.1016/j.eurpolymj.2023.112551.

[14] M. Ejaz, S.-W. Kuo, Solid state chemical transformation provides a fully benzoxazine-linked porous organic polymer displaying enhanced CO_2 capture and supercapacitor performance, Polym. Chem. 14 (2023) 2494–2509, https://doi.org/10.1039/D3PY00158J.

[15] K.I. Aly, S.M. Ebrahium, H.N. Abdelhamid, H.M. El-Bery, A.A.K. Mohammed, C. W. Huang, M.G. Mohamed, Efficient synthesis of main chain thermosetting polybenzoxazine resin containing tert-butylcyclohexanone and diphenylmethane units for supercapacitor energy storage, Eur. Polym. J. 221 (2024) 113519, https://doi.org/10.1016/j.eurpolymj.2024.113519.

[16] M.G. Mohamed, C.J. Li, M.A.R. Khan, C.C. Liaw, K. Zhang, S.W. Kuo, Formaldehyde-free synthesis of fully bio-based multifunctional bisbenzoxazine resins from natural renewable starting materials, Macromolecules 55 (2022) 3106–3115, https://doi.org/10.1021/acs.macromol.2c00417.

[17] C.-Y. Chen, W.-C. Chen, M.G. Mohamed, Z.-Y. Chen, S.-W. Kuo, Highly thermally stable, reversible, and flexible main chain type benzoxazine hybrid incorporating both polydimethylsiloxane and double-decker shaped polyhedral silsesquioxane units through diels–alder reaction, Macromol. Rapid Commun. 44 (2023) 2200910, https://doi.org/10.1002/marc.202200910.

[18] Y. Lu, N. Li, Y. Peng, M.G. Mohamed, S.-W. Kuo, K. Zhang, Facile and eco-friendly synthesis of hydrogen bonding-rich bio-based bisbenzoxazine resins with low surface free energy, strong adhesion strength and high thermal stability, Mol. Syst. Des. Eng. 9 (2024) 86–98, https://doi.org/10.1039/D3ME00066D.

[19] S. Sahu, B. Lochab, Sustainable benzoxazine-sulfur copolymer with dynamic linkages: recycling, reprocessing, self-healing, and shape recovery (R^2S^2), ACS Sustain. Chem. Eng. 12 (2024) 7126–7135, https://doi.org/10.1021/acssuschemeng.4c01317.

[20] C. Hu, Z. Yao, W. Zhao, K. Zhang, Synthesis, characterization, and structure–property investigations of benzoxazine resins with low surface free energy, Macromol. Chem. Phys. (2024) 2400152, https://doi.org/10.1002/macp.202400152.

[21] J. Chen, W. Bai, R. Jian, Y. Lin, X. Zheng, F. Wei, Q. Lin, F. Lin, Y. Xu, Molecular structure design of polybenzoxazines with low surface energy and low modulus for marine antifouling application, Prog. Org. Coat. 187 (2024) 108165, https://doi.org/10.1016/j.porgcoat.2023.108165.

[22] M. Zeng, H. Luo, Z. Feng, N. He, C. Tang, J. Chen, D. Zeng, Y. Zhou, Y. Shen, Structural design and polymerization of high-frequency low dielectric benzoxazine resins, ACS Appl. Polym. Mater. 6 (2024) 6614–6626, https://doi.org/10.1016/10.1021/acsapm.4c00891.

[23] X. Pan, M. Yuan, X. Lu, Z. Xin, Fluorine and silicon-containing main-chain type polybenzoxazine with low dielectric constant and high thermal stability, Polymer 300 (2024) 126995, https://doi.org/10.1016/j.polymer.2024.126995.

[24] H. Kimura, A. Matsumoto, K. Hasegawa, A. Fukuda, New thermosetting resin from bisphenol A-based benzoxazine and bisoxazoline, J. Appl. Polym. Sci. 72 (1999) 1551–1558, https://doi.org/10.1002/(SICI)1097-4628(19990620)72:12.

[25] H.Y. Low, H. Ishida, Mechanistic study on the thermal decomposition of polybenzoxazines: effects of aliphatic amines, J. Polym. Sci. Part B: Polym. Phys. 36 (1998) 1935–1946, https://doi.org/10.1002/(SICI)1099-0488(199808)36:11.

[26] M.G. Mohamed, W.-C. Chang, S.-W. Kuo, Crown ether- and benzoxazine-linked porous organic polymers displaying enhanced metal Ion and CO_2 capture through solid-state chemical transformation, Macromolecules 55 (2022) 7879–7892, https://doi.org/10.1021/acs.macromol.2c01216.

[27] M.M. Samy, M.G. Mohamed, T.H. Mansoure, T.S. Meng, M.A.R. Khan, C.-C. Liaw, S.-W. Kuo, Solid state chemical transformations through ring-opening polymerization of ferrocene-based conjugated microporous polymers in host–guest complexes with benzoxazine-linked cyclodextrin, J. Taiwan Inst. Chem. Eng. 132 (2022) 104110, https://doi.org/10.1016/j.jtice.2021.10.010.

[28] M.M. Samy, M.G. Mohamed, S.-W. Kuo, Pyrene-functionalized tetraphenylethylene polybenzoxazine for dispersing single-walled carbon nanotubes and energy storage, Compos. Sci. Technol. 199 (2020) 108360, https://doi.org/10.1016/j.compscitech.2020.108360.

[29] J. Liu, P. Guo, W. Yu, W. Zhao, K. Zhang, X. Liu, Direct conversion of liquid bio-benzoxazine precursor into porous graphene-based lubricant additive by laser irradiation, ACS Appl. Nano Mater. 7 (2024) 4355–4363, https://doi.org/10.1021/acsanm.3c05887.

[30] X.K. Li, B. Jiang, C. Wei, H.L. Lin, W. Zhao, K.Y. Ni, Y.X. Mu, J. Bian, D.Q. Chen, High-performance main-chain polybenzoxazine composites by incorporating multi-walled carbon nanotubes with different surfacial structure: mechanical properties, thermal stability and mechanisms, J. Appl. Polym. Sci. 140 (2023) e54482, https://doi.org/10.1002/app.54482.

[31] Q. Ran, W. Zhang, P. Li, Study on silicon-containing main chain type polybenzoxazines with both high heat resistance and low dielectric constant, Ind. Eng. Chem. Res. 62 (2023) 6158–6166, https://doi.org/10.1021/acs.iecr.3c00260.

[32] B. Akkus, H. Zhu, M. Mitsuishi, Bio-based benzoxazine-containing polycyclosiloxanes as flame-retardant adhesive materials, ACS Appl. Polym. Mater. 6 (2024) 9466–9476, https://doi.org/10.1021/acsapm.4c01105.

[33] S. Gulyuz, B. Kiskan, Combining siloxane-based polybenzoxazine with poly (ethylene-co-vinyl acetate/hydroxyl) for tougher, more stable, and self-healable materials, Eur. Polym. J. 212 (2024) 113073, https://doi.org/10.1016/j.eurpolymj.2024.113073.

[34] C.-W. Hsiao, A.M. Elewa, M.G. Mohamed, S.-W. Kuo, Highly stable hybrid porous polymers containing polyhedral oligomeric silsesquioxane (POSS)/Dibenzo[g,p] chrysene and Dibenzo[b,d]thiophene units for efficient Rhodamine B dye removal, Sep. Purif. Technol. 332 (2024) 125771, https://doi.org/10.1016/j.seppur.2023.125771.

[35] M.G. Mohamed, M. Hammad Elsayed, A.E. Hassan, A. Basit, I.M.A. Mekhemer, H.-H. Chou, K.-H. Chen, S.-W. Kuo, Hybrid porous polymers combination of octavinylsilsesquioxane/pyrene with benzothiadiazole units for robust energy storage and efficient photocatalytic hydrogen production from water, ACS Appl. Polym. Mater. 6 (2024) 5945–5956, https://doi.org/10.1021/acsapm.4c00655.

[36] Z.-Y. Chen, W.-C. Chen, S.-W. Kuo, Enhanced thermal and porous properties of double-decker-shaped polyhedral silsesquioxane-bismaleimide (DDSQ-BMI) nanocomposites for high-performance CO_2 storage and supercapacitors, Polym. Chem. 15 (2024) 553–564, https://doi.org/10.1039/D3PY01115A.

[37] T.-C. Chou, S.-W. Kuo, Controllable wet-brush blending of linear diblock copolymers with phenolic/DDSQ hybrids toward mesoporous structure phase diagram, Macromolecules 57 (2024) 5958–5970, https://doi.org/10.1021/acs.macromol.4c00665.

[38] D.-L. Zhou, J. Wang, H. Bai, D. Han, Q. Fu, High-performance low-k poly (dicyclopentadiene)-POSS nanocomposites achieved by frontal polymerization, Chem. Eng. J. 485 (2024) 150140, https://doi.org/10.1016/j.cej.2024.150140.

[39] L. Miao, L. Zhan, S. Liao, Y. Li, T. He, S. Yin, L. Wu, H. Qiu, The recent advances of polymer–POSS nanocomposites with low dielectric constant, Macromol. Rapid Commun. 45 (2024) 2300601, https://doi.org/10.1002/marc.202300601.

[40] S. Zhang, W. Chen, W. Hao, D. Li, C. Zhang, F. Yu, Y. Chen, A composite gel polymer electrolyte by incorporating modified POSS endowing inorganic-rich SEI formation and stable cycle life for lithium metal batteries, Chem. Eng. J. 484 (2024) 149499, https://doi.org/10.1016/j.cej.2024.149499.

[41] A. Basit, M.G. Mohamed, M. Ejaz, B.X. Su, H. Manzoor, S.W. Kuo, Boosting supercapacitor energy storage using microporous carbon derived from an octavinylsilsesquioxane and fluorenone-linked porous hybrid polymer, ACS Appl. Energy Mater. 7 (2024) 7505–7516, https://doi.org/10.1016/10.1021/acsaem.4c01796.

[42] M.G. Mohamed, S.W. Kuo, Functional silica and carbon nanocomposites based on polybenzoxazines, Macromol. Chem. Phys. 220 (2019) 1800306, https://doi.org/10.1002/macp.201800306.

[43] Y.C. Kao, W.C. Jing-Yu Lin, M.G. Chen, C.F. Mohamed, J.H.C. Huang, S.W. Kuo, High-thermal stable epoxy resin through blending nanoarchitectonics with double-decker-shaped polyhedral silsesquioxane-functionalized benzoxazine derivatives, Polymers 16 (2024) 112, https://doi.org/10.3390/polym16010112.

[44] C.W. Hsiao, A.M. Elewa, M.G. Mohamed, S.W. Kuo, Designing strategically functionalized hybrid porous polymers with octavinylsilsesquioxane/dibenzo[g,p] chrysene/benzo[c]-1,2,5-thiadiazole units for rapid removal of rhodamine B dye from water, Colloids Surf. A: Physicochem. Eng. Asp. 699 (2024) 134658, https://doi.org/10.1016/j.colsurfa.2024.134658.

[45] S.-W. Kuo, F.-C. Chang, POSS related polymer nanocomposites, Prog. Polym. Sci. 36 (2011) 1649–1696, https://doi.org/10.1016/j.progpolymsci.2011.05.002.

[46] D.B. Cordes, P.D. Lickiss, F. Rataboul, Recent developments in the chemistry of cubic polyhedral oligosilsesquioxanes, Chem. Rev. 110 (2010) 2081–2173, https://doi.org/10.1021/cr900201r.

[47] T. Pawlak, A. Kowalewska, B. Zgardzińska, M.J. Potrzebowski, Structure, dynamics, and host–guest interactions in POSS functionalized cross-linked nanoporous hybrid organic–inorganic polymers, J. Phys. Chem. C 119 (2015) 26575–26587, https://doi.org/10.1021/acs.jpcc.5b08868.

[48] K.J. Shea, D.A. Loy, B. Polysilsesquioxanes, Molecular-engineered hybrid organic–inorganic materials, Chem. Mater. 13 (2001) 3306–3319, https://doi.org/10.1021/cm011074s.

[49] H. Hu, Y. Zhang, Y. Hu, L. Xia, G. Li, Silver nanoparticles modified sulfur-containing POSS polymer membrane substrate for adsorption and surface-

enhanced Raman scattering analysis of chrysoidine in food samples, Talanta 271 (2024) 125653, https://doi.org/10.1016/j.talanta.2024.125653.

[50] X. Feng, K. Chen, X. Guo, J. Sun, Y. Jian, W. Yan, S. Qian, W. Xu, D. Chen, Structure-property relationship of polyhedral oligomeric silsesquioxanes/ polydimethylsiloxane superhydrophobic coatings for cotton fabrics, Prog. Org. Coat. 192 (2024) 108476, https://doi.org/10.1016/j.porgcoat.2024.108476.

[51] A. Kannan, C. Muthuraj, A. Mayavan, S. Gandhi, Multifaceted applications of polyhedral oligomeric silsesquioxane and their composites, Mater. Today Chem. 30 (2023) 101568, https://doi.org/10.1016/j.mtchem.2023.101568.

[52] M. Ejaz, M.M. Samy, Y. Ye, S.-W. Kuo, M. Gamal Mohamed, Design hybrid porous organic/inorganic polymers containing polyhedral oligomeric silsesquioxane/ pyrene/anthracene moieties as a high-performance electrode for supercapacitor, Int. J. Mol. Sci. 24 (2023) 2501, https://doi.org/10.3390/ijms24032501.

[53] M. Ejaz, M.G. Mohamed, S.U. Sharma, J.-T. Lee, C.-F. Huang, T. Chen, S.-W. Kuo, An ultrastable porous polyhedral oligomeric silsesquioxane/tetraphenylthiophene hybrid as a high-performance electrode for supercapacitors, Molecules 27 (2022) 6238, https://doi.org/10.3390/molecules27196238.

[54] M.-C. Tseng, Y.-L. Liu, Preparation, morphology, and ultra-low dielectric constants of benzoxazine-based polymers/polyhedral oligomeric silsesquioxane (POSS) nanocomposites, Polymer 51 (2010) 5567–5575, https://doi.org/10.1016/j.polymer.2010.09.040.

[55] Y.-C. Wu, S.-W. Kuo, Synthesis and characterization of polyhedral oligomeric silsesquioxane (POSS) with multifunctional benzoxazine groups through click chemistry, Polymer 51 (2010) 3948–3955, https://doi.org/10.1016/j.polymer.2010.06.033.

[56] K. Zhang, Q. Zhuang, X. Liu, G. Yang, R. Cai, Z. Han, A new benzoxazine containing benzoxazole-functionalized polyhedral oligomeric silsesquioxane and the corresponding polybenzoxazine nanocomposites, Macromolecules 46 (2013) 2696–2704, https://doi.org/10.1021/ma400243t.

[57] Y. He, A. Suliga, A. Brinkmeyer, M. Schenk, I. Hamerton, Effect of atomic oxygen exposure on polybenzoxazine/POSS nanocomposites for space applications, Compos. A 177 (2024) 107898, https://doi.org/10.1016/j.compositesa.2023.107898.

[58] N. Liu, L. Li, L. Wang, S. Zheng, Organic-inorganic polybenzoxazine copolymers with double decker silsesquioxanes in the main chains: synthesis and thermally activated ring-opening polymerization behavior, Polymer 109 (2017) 254–265, https://doi.org/10.1016/j.polymer.2016.12.049.

[59] Y.-T. Liao, Y.-C. Lin, S.-W. Kuo, Highly thermally stable, transparent, and flexible polybenzoxazine nanocomposites by combination of double-decker-shaped

polyhedral silsesquioxanes and polydimethylsiloxane, Macromolecules 50 (2017) 5739–5747, https://doi.org/10.1021/acs.macromol.7b01085.

[60] P. Wang, S. Zhang, W. Xu, T. Xiao, Q. Ran, High heat-resistant and degradable polybenzoxazines with a diacetal structure, ACS Sustain. Chem. Eng. 9 (2021) 7913–7921, https://doi.org/10.1021/acssuschemeng.1c01919.

[61] W.C. Chen, S.W. Kuo, Ortho-imide and allyl groups effect on highly thermally stable polybenzoxazine/double-decker-shaped polyhedral silsesquioxane hybrids, Macromolecules 51 (2018) 9602–9612, https://doi.org/10.1021/acs.macromol.8b02207.

[62] Y. Xing, X. He, R. Yang, K. Zhang, S. Yang, Design of high-performance polybenzoxazines with tunable extended networks based on resveratrol and allyl functional benzoxazine, Polymers 12 (2020) 2794, https://doi.org/10.3390/polym12122794.

[63] Y. Xia, L. Liu, L. Wang, R. Shi, S. Yan, X. Zhao, Y. Sheng, Z. Wang, Synthesis, polymerization kinetics of 4-allyl-substituted 1,3-benzoxazine and properties of resulting polymer, Thermochim. Acta 717 (2022) 179350, https://doi.org/10.1016/j.tca.2022.179350.

[64] S. Mukherjee, B. Lochab, Hydrogen bonding-guided strategies for thermal performance modulation in biobased oxazine ring-substituted benzoxazine thermosets, Macromolecules 57 (2024) 1795–1807, https://doi.org/10.1016/10.1021/acs.macromol.3c02454.

[65] L. Zhao, C. Zhao, M. Wu, Y. Li, H. Li, D. Xiang, C. Guo, Curing kinetics of phenolphthalein based polyphosphazene towards thermal stability and flame retardancy of polybenzoxazine, RSC Adv. 9 (2019) 31583–31593, https://doi.org/10.1039/C9RA06857K.

[66] M.G. Mohamed, S.-W. Kuo, Progress in the self-assembly of organic/inorganic polyhedral oligomeric silsesquioxane (POSS) hybrids, Soft Matter 18 (2022) 5535–5561, https://doi.org/10.1016/10.1039/D2SM00635A.

[67] M.G. Mohamed, T.H. Mansoure, Y. Takashi, M. Mohamed Samy, T. Chen, S.-W. Kuo, Ultrastable porous organic/inorganic polymers based on polyhedral oligomeric silsesquioxane (POSS) hybrids exhibiting high performance for thermal property and energy storage, Microporous Mesoporous Mater. 328 (2021) 111505, https://doi.org/10.1016/j.micromeso.2021.111505.

[68] J. Lyu, B. Ji, N. Wu, W. Liao, C. Yin, S. Bai, S. Xing, The effect of substituent group in allyl benzoxazine on the thermal, mechanical and dielectric properties of modified bismaleimide, React. Funct. Polym. 191 (2023) 105673, https://doi.org/10.1016/j.reactfunctpolym.2023.105673.

[69] X. Wang, B. Liu, D. Chen, D. Zhang, X. Li, J. He, R. Yang, Molecular-level fabrication strategies for the POSS cross-linked polybenzoxazines, J. Polym. Sci. 61 (2023) 1634–1650, https://doi.org/10.1002/pol.20230052.